Brillouin Optical Microscopy for Corneal Biomechanics

Giuliano Scarcelli,[1,2] *Roberto Pineda,*[3] *and Seok Hyun Yun*[1,2,4]

Purpose. The mechanical properties of corneal tissue are linked to prevalent ocular diseases and therapeutic procedures. Brillouin microscopy is a novel optical technology that enables three-dimensional mechanical imaging. In this study, the feasibility of this noncontact technique was tested for in situ quantitative assessment of the biomechanical properties of the cornea.

Methods. Brillouin light-scattering involves a spectral shift proportional to the longitudinal modulus of elasticity of the tissue. A 532-nm single-frequency laser and a custom-developed ultrahigh-resolution spectrometer were used to measure the Brillouin frequency. Confocal scanning was used to perform Brillouin elasticity imaging of the corneas of whole bovine eyes. The longitudinal modulus of the bovine corneas was compared before and after riboflavin corneal collagen photo-cross-linking. The Brillouin measurements were then compared with conventional stress–strain mechanical test results.

Results. High-resolution Brillouin images of the cornea were obtained, revealing a striking depth-dependent variation of the elastic modulus across the cornea. Along the central axis, the Brillouin frequency shift varied gradually from 8.2 GHz in the epithelium to 7.5 GHz near the endothelium. The coefficients of the down slope were measured to be approximately 1.09, 0.32, and 2.94 GHz/mm in the anterior, posterior, and innermost stroma, respectively. On riboflavin collagen cross-linking, marked changes in the axial Brillouin profiles ($P < 0.001$) were noted before and after cross-linking.

Conclusions. Brillouin imaging can assess the biomechanical properties of cornea in situ with high spatial resolution. This novel technique has the potential for use in clinical diagnostics and treatment monitoring. (*Invest Ophthalmol Vis Sci.* 2012; 53:185–190) DOI:10.1167/iovs.11-8281

The current standard of corneal diagnosis is structural analysis, by pachymetry[1] and tomography,[2] to measure corneal thickness and curvature. In addition to structure, the biomechanical properties of the cornea are also important indicators of corneal health. Keratoconus is a degenerative condition that involves a loss of corneal rigidity. Corneal ectasia, which can occur as a rare but serious complication of refractive surgery, results from a decrease in corneal stiffness. Corneal cross-linking is a procedure that increases the elastic modulus of the cornea to prevent ectasia.[3–5] It has been used in the treatment of keratoconus and ectasia after refractive surgery. A noninvasive device that could measure corneal biomechanical properties[3] would be highly useful in the clinic.[6]

Most of our current knowledge on the mechanical properties of the cornea came from modeling[7] or ex vivo experimental studies performed with stress–strain tests,[8] dynamic rheometry, and other mechanical tests.[9,10] As the compelling clinical need of biomechanical information has increased,[6] various in vivo techniques have been under active development. The ocular response analyzer[11] (ORA; Reichert, DePew, NY) uses an air puff to induce pressure on the corneal surface and optically measures the time-dependent deformation of the cornea. However, its sensitivity and clinical usefulness remain questionable.[12–14] Several elastography techniques are currently under development.[15–18] Ultrasound has long been investigated,[19] but thus far is difficult to use in vivo because of its low sensitivity and resolution. However, more sophisticated techniques such as quantitative ultrasound spectroscopy continue to be investigated.[20]

In this context, we have recently developed a novel technique termed Brillouin optical microscopy that can measure the viscoelastic properties by probing the hypersonic acoustic waves inherently present in the sample.[21] Like ultrasound spectroscopy, Brillouin microscopy can determine intrinsic viscoelastic properties decoupled from the structural information and applied pressure. In contrast, it can measure the local acoustic properties with much higher spatial resolution and sensitivity, and the measurement is performed optically without the need for acoustic transducers or physical contact with the cornea. Vaughan and Randall[22] have measured the Brillouin spectra of excised cornea and lens. The conventional Brillouin instruments had extremely slow data acquisition, requiring 10 to 60 minutes to obtain a single Brillouin spectrum. Brillouin microscopy drastically improved the data acquisition time to less than a second,[23] allowing spatially resolved analysis.

We report our investigation of corneal biomechanics using Brillouin microscopy. For this work, we constructed a tabletop instrument combining a simple confocal microscope with a high-speed spectrometer. Using Brillouin microscopy on fresh bovine whole eyes ex vivo, we showed, to our knowledge for the first time in situ, the ability to image corneal elasticity in three dimensions and measure the depth-dependent variation of elastic modulus within the cornea. We also demonstrate the feasibility of monitoring riboflavin-assisted corneal cross-linking procedures, using Brillouin microscopy.

Materials and Methods

Brillouin Elastic Modulus

Brillouin light-scattering arises from the interaction of incident light with propagating thermodynamic fluctuations, also known as acoustic phonons, in the sample material. The Brillouin-scattered light is characterized by a frequency shift, Ω, which is related to the longitudinal elastic modulus, M' (the real part of complex modulus), of the sample via[23–25]

From the [1]Wellman Center for Photomedicine, Massachusetts General Hospital, Boston, Massachusetts; the [2]Department of Dermatology, Harvard Medical School, Boston, Massachusetts; the [3]Department of Ophthalmology, Massachusetts Eye and Ear Infirmary, Boston, Massachusetts; and [4]Harvard-MIT Health Sciences and Technology, Cambridge, Massachusetts.

Supported by a Tosteson Fellowship (GS), Grant R21EB008472 from the National Institutes of Health, and Grant CBET-0853773 from the National Science Foundation.

Submitted for publication July 23, 2011; revised September 8, October 1, and November 3, 2011; accepted November 28, 2011.

Disclosure: **G. Scarcelli**, None; **R. Pineda**, None; **S.H. Yun**, None

Corresponding author: Seok Hyun Yun, Department of Dermatology, Harvard Medical School, 55 Fruit Street, Boston, MA 02114; syun@hms.harvard.edu.

$$M' = 1/4\Omega^2\lambda^2(\rho/n^2) \quad (1)$$

where λ is the optical wavelength in air, ρ is the mass density, and n is the refractive index. Although the structural and optical properties of the cornea are generally anisotropic, our measurements of Brillouin frequency shifts indicated negligible dependence on the optical polarization state, compared to their variation over depth in the cornea. Brillouin microscopy measures the frequency shift by employing an ultrahigh-resolution spectrometer. In the case of backscattering of visible light, the Brillouin frequency shift is approximately 5 to 15 GHz in soft tissues, and the corresponding longitudinal modulus ranges typically from 2 to 6 GPa.

The conversion from the Brillouin shift to the elastic modulus requires the knowledge of the index–density factor ρ/n^2. Both refractive index and density are not uniform in the cornea, mainly because of the spatial variations of hydration[26,27] and water/protein content.[28,29] Treating the cornea as an aqueous solution of collagen fibers and extrafibrillar material with spatially varying concentrations,[30,31] we can write $n = 1.335 + 0.04/(0.22 + 0.24H)$, where corneal hydration (weight%) H ranges from 3 to 4 in normal corneas,[31–33] and $\rho = (\rho_T + H)/(1 + H)$ where $\rho_T = 1.33$ is the density of dry tissue.[34] From the formulas, we calculate: $n = 1.3689–1.3775$, $\rho = 1.066–1.083$ g/cm^3, and $\rho/n^2 = 0.569–0.571$ g/cm^3. In ρ/n^2, the index and density changes cancel each other, and the resultant variation of ρ/n^2 is ~0.3% in the cornea. Ignoring this small variation, we used a constant value of 0.57 g/cm^3 for ρ/n^2 in our analysis.

Brillouin Confocal Microscope

Figure 1a illustrates the experimental setup. We used a frequency-doubled Nd-YAG laser (Torus; Laser Quantum, Inc., San Jose, CA) emitting a single-mode laser line with a line width of 1 MHz at 532 nm. The beam was expanded and aligned into an inverted microscope setup using an objective lens (focal length of 16 mm, numerical aperture of 0.25; Edmund Optics, Barrington, NJ), which resulted in a spatial resolution of ~$1 \times 1 \times 5$ μm^3 (in x-y-z). The laser power on the sample was typically 7 to 15 mW. A custom-made sample-holding chamber was mounted on a three-axis motorized stage (Zaber Technologies, Vancouver, BC, Canada, and NewFocus; Newport Corp., Santa Clara, CA). The scattered light from the sample was collected by a single-mode optical fiber (Thorlabs, Newton, NJ) and delivered to a two-stage VIPA (virtually imaged phase array) spectrometer with sub-GHz frequency resolution.[35] The spectrometer was constructed with two VIPA etalons in the cross-axis configuration.[36] The dispersed optical spectrum was recorded by using an EM-CCD camera (Ixon Du197; Andor, Belfast, Northern Ireland, UK) with a frame integration time of 250 ms.

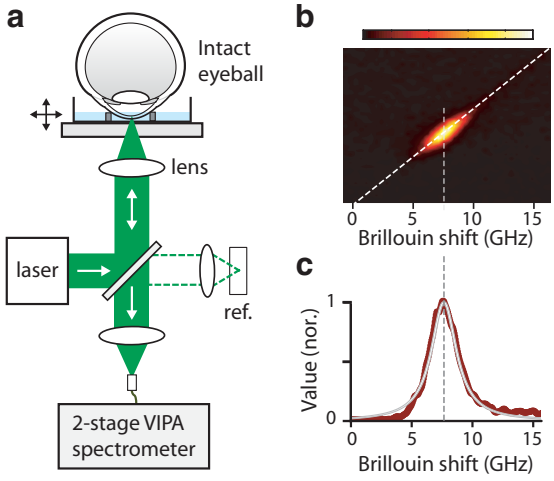

Figure 1. Brillouin optical microscopy. (**a**) The inverted microscope setup. (**b**) A typical CCD output of the spectrometer, showing the Brillouin spectrum of a corneal stroma. (**c**) Analysis of the Brillouin spectrum (*red trace*) with Lorentzian curve fit (*gray trace*).

Data Acquisition and Analysis

A software program (LabVIEW; National Instruments, Austin TX) was implemented for the synchronous control of the translational stages, CCD camera, and data-acquisition board. Figure 1b shows a CCD frame featuring the typical Brillouin signal from the cornea. The corresponding Brillouin spectrum (red) was then analyzed with Lorentzian curve fit (gray) by using a custom-written program (MatLab; The MathWorks, Natick, MA) to determine the Brillouin frequency shift (Fig. 1c). For imaging, the control software moved the motorized stage at constant speeds in the x, y, and z planes, as the Brillouin spectrum at each location was recorded continuously with the CCD camera. A Brillouin image of the sample was produced by plotting the measured frequency shifts over space with color encoding. The scan speed of the sample stage and the CCD frame integration time determine the spatial interval between pixels in the Brillouin image.

Cornea Samples

Bovine whole eyes (~1 year old) were obtained 2 to 4 hours postmortem (Research 87, Inc., Boylston, MA). Whole eyes were placed in the chamber holder. The chamber was filled with isotonic solution or mineral oil to prevent drying of the cornea and maintain the transparency during measurement. After imaging, we surgically extracted the cornea, fixed it in 10% formalin, and cut 5-μm-thick slices from the central region for histologic analysis. H&E staining was used for standard structural examination. For collagen analysis, we used Masson's trichrome staining and performed second-harmonic generation microscopy with unstained sections after deparaffinization.

Corneal Collagen Cross-Linking

The corneal epithelium of the bovine eye was removed by a 1-minute soak in 20% ethanol solution followed by gentle scraping with a blade (Parker 15; BD Biosciences, San Diego, CA). Riboflavin (riboflavin-5-phosphate; Sigma-Aldrich, St. Louis, MO) was diluted in PBS to a riboflavin solution of 0.1%. The corneas without epithelium were fully soaked in the riboflavin solution for 5 minutes. Excess riboflavin on the tissue surface was washed away with PBS. The corneas were then exposed to a Xenon lamp (λ = 460 nm, 15 mW/cm^2) for 20 minutes. During irradiation, a drop of riboflavin solution was applied to the cornea every 5 minutes. After corneal cross-linking, the whole eyes were placed in the chamber holder for Brillouin measurements.

Measurement of Young's Modulus

After Brillouin imaging, we cut 5-mm-diameter disks out of the sample using a biopsy punch and performed compressive stress–strain tests at constant strain rates (1% strain per minute) using a standard instrument (model 5542; Instron, Norwood, MA). The stress–strain response curves of all the cornea specimens showed typical J-shaped profiles.[37] Young's modulus was calculated from the slope of linear regression of the stress–strain curves in the range between 1% and 10% strain excluding the initial region below 1% strain.

Results

Mapping Corneal Elasticity in Three Dimensions

Figure 2a shows the cross-sectional image of the anterior segment of a normal bovine eye (cornea) (in the x–z plane). The Brillouin image revealed a distinct spatial variation of Brillouin frequency shift (cf. elastic modulus). Most notably, the Brillouin frequency shift was the highest in the anterior corneal region but decreased gradually toward the endothelium. The Brillouin shift in the aqueous humor is similar to that of pure water (~7.5 GHz). Compared to the depth (axial) variation,

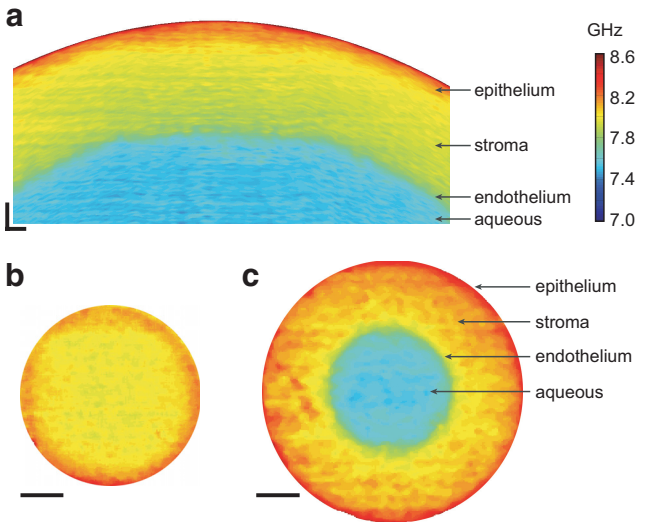

Figure 2. Brillouin imaging of the cornea. (**a**) A cross-sectional Brillouin image of bovine cornea, revealing the decreasing modulus with depth. The horizontal (x) and vertical (z) span is 5 × 0.5 mm. (**b**) En face Brillouin image of the cornea optically sectioned at a shallow depth. (**c**) A Brillouin image of a deeper section. Scale bars: (**a**) 200 μm; (**b**, **c**) 1 mm.

there was much less variation laterally at the same depth from the corneal surface. Figures 2b and 2c show en face Brillouin images of the same sample acquired along two horizontal planes (x–y) as the eye was moved horizontally with respect to the laser beam. A high degree of radial symmetry is observed in the en face images throughout all depths.

Brillouin Profiles and Microstructure

Most of the corneal stroma consists of 200 to 500 layers of flattened collagenous lamellae. Collagen fibril organization is responsible for the mechanical strength of corneal stroma.[38–40] In the anterior one third of the stroma, collagen lamellae are thin (~0.2–1.2 μm thick and 0.5–30 μm wide) and are positioned obliquely to the corneal surface, sometimes interwoven. In the posterior stroma, collagen lamellae tend to be arranged parallel to the surface and are thicker (1.0–2.5 μm thick and 100 to 250 μm wide).[41] To investigate the correlation between the structure and elastic modulus of the cornea, we compared a high-resolution axial profile of an intact cornea (Fig. 3a) with a collagen-stained (Masson's trichrome) image of the corresponding corneal section (Fig. 3b). From the side-by-side comparison, we identified four distinctive regions: (I) the epithelial region with low elastic modulus; (II) the anterior part of the stroma characterized by the highest elastic modulus and a steep downslope of the Brillouin modulus; (III) the posterior region with a mild downslope; and (IV) the innermost region near the endothelium, where the modulus decreases rapidly with depth. The anterior (II) and posterior (III) regions in the Brillouin image seem to correlate with the description of the two regions with distinctively different collagen structures.[40]

To examine the microstructure, we performed second-harmonic generation (SHG) microscopy of an unstained tissue section harvested from the same cornea (Fig. 3c). Consistent with previous observations in human, rabbit, and porcine corneas,[42–44] the SHG image of bovine cornea visualized the collagen-rich structure in the stroma but little collagen in the epithelium. The anterior part of the stroma shows a markedly interwoven and intertwined organization of collagen fibers. In the posterior and innermost region of the cornea, collagen fibers mostly run parallel to the corneal surface. The qualitative correlation between the magnitudes of Brillouin frequency shift, and the SHG signal supports the hypothesis that the collagen content and fibril organization may be the principal determining factor of corneal elasticity.[40]

Axial Slopes and Mean Modulus

We measured the axial slopes in the anterior, posterior, and innermost corneal regions (N = 4). In the anterior region between 80 and 180 μm from the corneal surface, the average slope was 1.09 ± 0.26 GHz/mm (ignoring the negative sign of the slope); in the posterior region between 300 and 550 μm, the slope was 0.32 ± 0.1 GHz/mm; and in the innermost region between 680 and 780 μm, we measured a slope of 2.94 ± 0.18 GHz/mm (Fig 4a). The Brillouin slope of each region was statistically distinct (unpaired t-test $P < 0.001$ for all two-group comparisons). The mean longitudinal modulus of the four tested samples was 2.7 ± 0.02 GPa (Fig. 4b).

Brillouin Imaging of Corneal CXL

Next, we evaluated the potential of Brillouin imaging to monitor corneal CXL. CXL promotes the formation of covalent bonds between collagen fibers in the stroma by optical activation of a biocompatible photosensitizing agent such as riboflavin. Previous stress–strain and inflation tests[45,46] established that the induced cross links between collagen fibers increase the elastic modulus of the corneal tissue, thereby stiffening the cornea. We measured the Brillouin modulus on bovine corneal samples during the CXL procedure performed with riboflavin

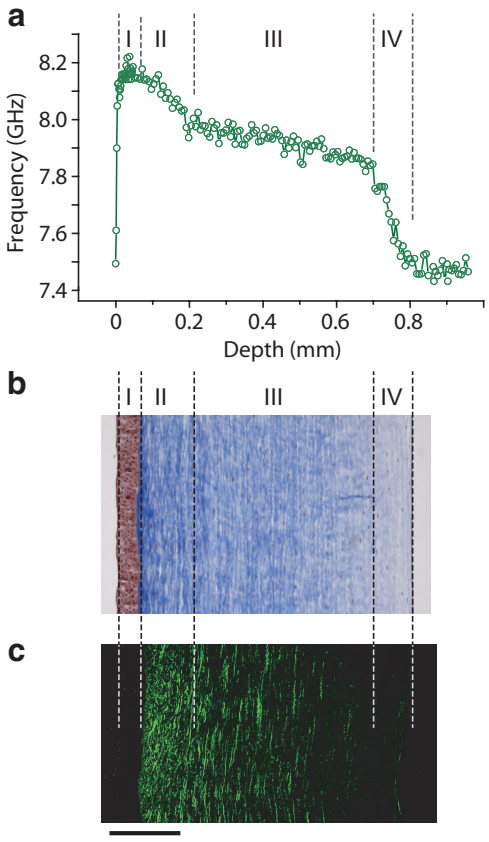

Figure 3. Comparison of Brillouin elasticity and structural images. (**a**) Brillouin depth profile of the entire cornea including the epithelium (I), anterior stroma (II), posterior stroma (III), and the innermost region (IV). (**b**) Masson's trichrome–stained image of 5-μm-thick cornea section. (**c**) An SHG image of 5-μm-thick cornea section. Scale bar, 200 μm.

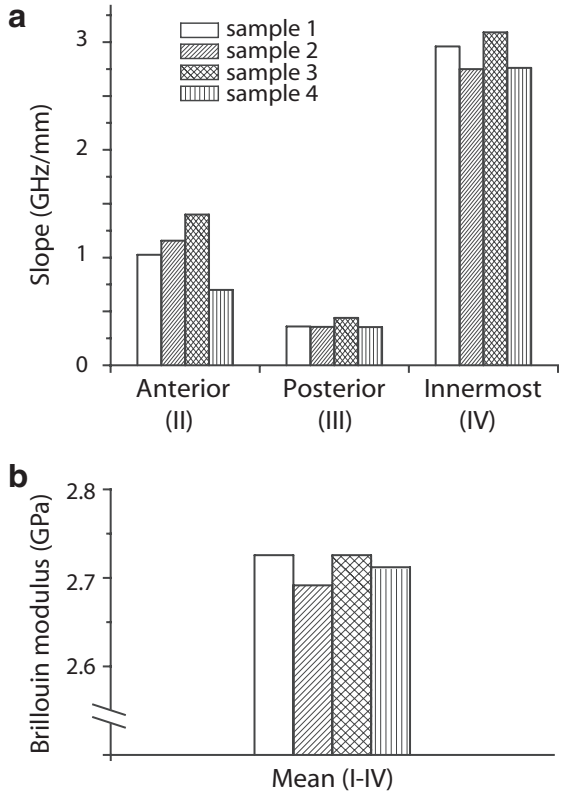

Figure 4. Brillouin axial slopes and mean modulus. (**a**) Downslope coefficients in the anterior (II), posterior (III), and innermost (IV) regions of the stroma. (**b**) The mean Brillouin modulus for the entire depth (I–IV).

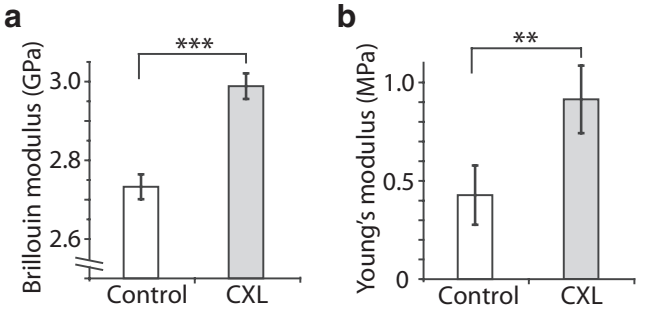

Figure 6. Comparison of Brillouin modulus and Young's modulus. (**a**) Mean Brillouin modulus of normal versus CXL-treated corneas. (**b**) Young's modulus of normal versus CXL-treated corneas. Error bars, SD ($n = 4$). $^{***}P < 0.001$; $^{**}P < 0.03$.

and blue light (see the Methods section). Figure 5 shows Brillouin cross-sectional images of a de-epithelialized bovine cornea sample before (Fig. 5a) and after (Fig. 5b) the CXL procedure. It is apparent that the cross-linking procedure resulted in a substantial increase of Brillouin modulus in the stroma. The shrinking of corneal thickness was noticeable, consistent with previous observations.[47]

Figure 5c shows the typical Brillouin axial profiles of a few corneal samples measured at various stages of the CXL procedure. We found that the Brillouin frequency shifts were not altered by the removal of the epithelium (red circles) or by soaking in riboflavin solution before illumination with blue light (green circles). However, after optical irradiation, there were dramatic changes in the Brillouin profiles (orange, cyan, and blue data points). The increase in Brillouin frequency was almost universal across the entire stroma (except for the innermost region). The magnitude of change decreased almost linearly with the depth, probably due to the depth-dependent gradient of riboflavin concentration and intensity of activation light.[48] The Brillouin slope of the cross-linked samples was 1.5 ± 0.16 GHz/mm, an increase of almost sixfold from 0.25 ± 0.1 GHz/mm before cross-linking (Fig. 5d, unpaired *t*-test $P < 0.001$).

Comparison with Standard Mechanical Measurements

To compare the Brillouin modulus to Young's modulus, we performed Brillouin imaging and standard stress–strain tests[49] in two sample groups: untreated and CXL-treated corneas ($N = 4$ each). After Brillouin measurements, we resected a central corneal button from each sample and measured the linear slope of its stress–strain curve. The Brillouin moduli of the control and treated groups were 2.7 ± 0.03 GPa and 2.98 ± 0.03 GPa, respectively (Fig. 6a). The increase in the Brillouin modulus with CXL was only approximately 10% but was statistically significant (unpaired *t*-test, $P < 0.001$). By comparison, the Young's moduli of the control group was 0.4 ± 0.1 MPa and that of the CXL-treated group was 0.9 ± 0.2 MPa (Fig. 6b), about a twofold increase after CXL (unpaired *t*-test, $P = 0.03$).

The Brillouin longitudinal modulus and Young's modulus are based on different mechanisms by which the pressure is applied. As previously described,[23] the difference in magnitude between the two moduli of elasticity comes primarily from their different physical definitions and also from the different time scales of pressure modulation (GHz for acoustic phonons and Hz for mechanical stress). However, despite the apparent difference in absolute scale, the experimental data suggest a quantitative correlation between these two moduli of elasticity

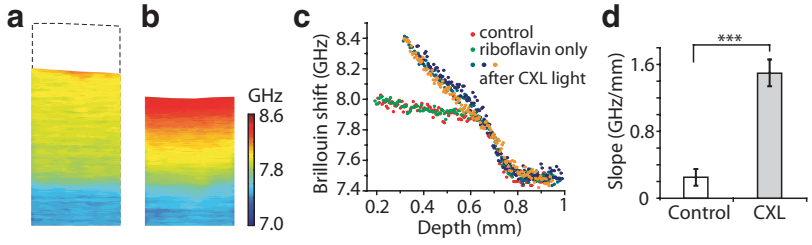

Figure 5. Brillouin measurement of the CXL procedure. (**a**) A cross-sectional (*x-z*) Brillouin image of untreated cornea without the epithelium. (**b**) A Brillouin image of the cornea after CXL treatment. (**c**) Brillouin depth profiles of the de-epithelialized cornea before treatment, after Riboflavin soaking, and after illumination of the treatment light (*orange*, *cyan*, and *blue circles*). (**d**) The slope of the Brillouin frequency in the stroma before and after the CXL treatment. Error bars, SD ($n = 4$). $^{***}P < 0.001$.

for the cornea. We note that the noncontact, high-resolution nature of Brillouin imaging provided less sample-to-sample variation and better measurement repeatability, resulting in significantly more clear separation between the two sample groups.

Discussion

In this study, we present novel Brillouin optical microscopy that can provide quantitative microscopic information on corneal elasticity in vitro. Brillouin imaging visualized the spatially heterogeneous biomechanical properties of the cornea.[50] It revealed a marked depth-dependent variation in elastic modulus from the epithelium through the stroma to the endothelium. We observed the anterior portion of the stroma to have the highest elastic modulus in the cornea. This observation is consistent with previous conventional mechanical measurements and the analysis of collagen microstructure. Kohlhaas et al.[51] reported that the anterior part of the stroma has nearly three times higher elastic moduli than the posterior part of the stroma. Muller et al.[52] showed that the tightly interwoven collagen fiber network in the anterior stroma is mainly responsible for the structural integrity of the cornea. Recently, Randleman et al.[53] performed tensile stress–strain tests on shaved-off corneal layers and found an interestingly similar trend of decreasing elastic modulus across the corneal depth. From the Brillouin images of normal bovine corneas, we defined and measured the axial slopes and mean Brillouin modulus, parameters that may serve as useful quantitative metrics of corneal biomechanics.

We also demonstrated the feasibility of Brillouin imaging as a tool for monitoring CXL treatment in patients with keratoconus or corneal ectasia. Brillouin imaging can be used to measure the degree of cross-linking with high spatial and temporal resolutions, providing information about the diffusion kinetics of the photo-cross-linking compounds and light intensity distribution. This possibility may prove useful in the preclinical setting for developing new photo-cross-linking compounds and optimizing the CXL procedure.

Our results validated Brillouin modulus with respect to Young's modulus measured by a conventional compressive stress–strain test. For a given tissue sample, the Brillouin longitudinal moduli are considerably higher than Young's moduli for fundamental reasons: First, the cornea consists primarily of water (>75%). As a result, the longitudinal modulus of tissue is on the same order of magnitude as the bulk modulus (2.2 GPa) of incompressible water (Poisson's ratio, ~0.5). Nevertheless, our data suggest that the deviation of Brillouin modulus of corneal tissue from the bulk modulus of pure water can be an accurate and useful measure of the mechanical properties of the tissue. Second, the elastic modulus tends to increase with frequency,[54] as many relaxation processes have little time to respond to fast mechanical or acoustic modulation. Despite the large difference in the time scale, there seems to be a good correlation between the Brillouin modulus and Young's modulus of soft tissue.[23] This finding suggests that Brillouin microscopy can be used not only for comparative study but also for quantitative analysis, especially after calibration with standard mechanical tests for the given type of sample.

The mechanical balance between corneal stiffness and IOP is critical in maintaining the normal structure and function of the cornea. Corneal stiffness, the resistance to IOP, comes from both the corneal thickness and the elastic moduli of the tissues that constitute the cornea. Although the corneal thickness can be measured accurately by pachymetry and topography, currently no clinical device is capable of reliably measuring the elastic modulus and the stiffness of the cornea in vivo. Brillouin optical microscopy is capable of measuring the intrinsic material property of the cornea, independently of the corneal thickness and the IOP. The accurate measurement of IOP is important in the diagnosis of glaucoma and in monitoring the effectiveness of medication, but current applanation tonometry has several known error sources. Studies suggested that the variation of corneal modulus of elasticity may be the major confounding factor.[33] Brillouin microscopy can potentially allow more accurate determination of IOP, improving the diagnosis and management of glaucoma-suspect patients.

In conclusion, we have presented a novel imaging technology, Brillouin optical microscopy, capable of mapping the elastic modulus of cornea noninvasively with three-dimensional resolution. Our results suggest several potential applications such as early detection of keratoconus and corneal ectasia as well as monitoring of corneal cross-linking procedures. We are currently developing a Brillouin optical scanner suitable and safe for use in humans. Such an instrument with the capability of mapping corneal biomechanical properties may prove clinically useful.

Acknowledgments

The authors thank Irene E. Kochevar for helpful discussions, Robert Langer and Jason Nichols (Massachusetts Institute of Technology) for providing access to the mechanical test equipment, Konrad Sawicki for help with cross-linking measurements, and the Histopathology Lab at Wellman Center for help with histology analysis.

References

1. Marsich MM, Bullimore MA. The repeatability of corneal thickness measures. *Cornea.* 2000;19:792–795.
2. Izatt JA, Hee MR, Swanson EA, et al. Micrometer-scale resolution imaging of the anterior eye in-vivo with optical coherence tomography. *Arch Ophthalmol.* 1994;112:1584–1589.
3. Ethier CR, Johnson M, Ruberti J. Ocular biomechanics and biotransport. *Ann Rev Biomed Eng.* 2004;6:249–273.
4. Wollensak G. Crosslinking treatment of progressive keratoconus: new hope. *Curr Opin Ophthalmol.* 2006;17:356–360.
5. Pepose JS, Feigenbaum SK, Qazi MA, Sanderson JP, Roberts CJ. Changes in corneal biomechanics and intraocular pressure following LASIK using static, dynamic, and noncontact tonometry. *Am J Ophthalmol.* 2007;143:39–47.
6. Roberts C. The cornea is not a piece of plastic. *J Refractive Surg.* 2000;16:407–413.
7. Pandolfi A, Holzapfel GA. Three-dimensional modeling and computational analysis of the human cornea considering distributed collagen fibril orientations. *J Biomech Eng.* 2008;130:061006.
8. Hoeltzel DA, Altman P, Buzard K, Choe KI. Strip extensiometry for comparison of the mechanical response of bovine, rabbit, and human corneas. *J Biomech Eng.* 1992;114:202–215.
9. Woo SL, Kobayashi AS, Schlegel WA, Lawrence C. Nonlinear material properties of intact cornea and sclera. *Exp Eye Res.* 1972; 14:29–39.
10. Vogel A, Capon MRC, Asiyovogel MN, Birngruber R. Intraocular photodisruption with picosecond and nanosecond laser-pulses: tissue effects in cornea, lens and retina. *Invest Ophthalmol Vis Sci.* 1994;35:3032–3044.
11. Luce DA. Determining in vivo biomechanical properties of the cornea with an ocular response analyzer. *J Cataract Refract Surg.* 2005;31:156–162.
12. Ang GS, Nicholas S, Wells AP. Poor utility of intraocular pressure correction formulae in individual glaucoma and glaucoma suspect patients. *Clin Exp Ophthalmol.* 2011;39:111–118.
13. Fontes BM, Ambrosio R Jr, Velarde GC, Nose W. Ocular response analyzer measurements in keratoconus with normal central corneal thickness compared with matched normal control eyes. *J Refract Surg.* 2011;27:209–215.
14. Kotecha A. What biomechanical properties of the cornea are relevant for the clinician? *Surv Ophthalmol.* 2007;52:S109–S114.

15. Ambrosio R Jr, Caldas D, Ramos I, Santos R, Belin, M. *Corneal Biomechanical Assessment Using Dynamic Ultra High-Speed Scheimpflug Technology Non-contact Tonometry (UHS-ST NCT): Preliminary Results.* Presented at the American Society of Cataract and Refractive Surgery-American Society of Ophthalmic Administrators (ASCRS-ASOA) Symposium and Congress. San Diego, CA, March 25–29, 2011.
16. Ford MR, Dupps WJ Jr, Rollins AM, Roy AS, Hu, Z. Method for optical coherence elastography of the cornea. *J Biomed Opt*. 2011;16:016005.
17. Grabner G, Ellmsteiner R, Steindl C, Ruckhofer J, Mattioli R, Husinsky W. Dynamic corneal imaging. *J Cataract Refract Surg.* 2005; 31:163–174.
18. Tanter M, Touboul D, Gennisson J-L, Bercoff J, Fink M. High-resolution quantitative imaging of cornea elasticity using supersonic shear imaging. *IEEE Trans Med Imaging.* 2009;28:1881–1893.
19. Wang HC, Prendiville PL, McDonnell PJ, Chang WV. An ultrasonic technique for the measurement of the elastic moduli of human cornea. *J Biomech.* 1996;29:1633–1636.
20. He X, Liu J. A quantitative ultrasonic spectroscopy method for noninvasive determination of corneal biomechanical properties. *Invest Ophthalmol Vis Sci.* 2009;50:5148–5154.
21. Scarcelli G, Yun SH. Confocal Brillouin microscopy for three-dimensional mechanical imaging. *Nat Photonics.* 2008;2:39–43.
22. Vaughan JM, Randall JT. Brillouin scattering, density and elastic properties of the lens and cornea of the eye. *Nature.* 1980;284: 489–491.
23. Scarcelli G, Kim P, Yun SH. In vivo measurement of age-related stiffening in the crystalline lens by Brillouin optical microscopy. *Biophys J.* 2011;101:1539–1545.
24. Randall J, Vaughan JM. The measurement and interpretation of Brillouin scattering in the lens of the eye. *Proc R Soc Lond Series B Biol Sci.* 1982;214:449–470.
25. Reiss S, Burau G, Stachs O, Guthoff R, Stolz H. Spatially resolved Brillouin spectroscopy to determine the rheological properties of the eye lens. *Biomed Opt Express.* 2011;2:2144–2159.
26. Kikkawa Y, Hirayama K. Uneven swelling of corneal stroma. *Invest Ophthalmol* 1970;9:735–741.
27. Wilson G, Oleary DJ, Vaughan W. Differential swelling in compartments of the corneal stroma. *Invest Ophthalmol Vis Sci.* 1984;25: 1105–1108.
28. Vasudevan B, Simpson TL, Sivak JG. Regional variation in the refractive-index of the bovine and human cornea. *Optom Vis Sci.* 2008;85:977–981.
29. Castoro JA, Bettelheim AA, Bettelheim FA. Water gradients across bovine cornea. *Invest Ophthalmol Vis Sci.* 1988;29:963–968.
30. Patel S, Alio JL, Perez-Santonja JJ. Refractive index change in bovine and human corneal stroma before and after LASIK: a study of untreated and re-treated corneas implicating stromal hydration. *Invest Ophthalmol Vis Sci.* 2004;45:3523–3530.
31. Meek KM, Dennis S, Khan S. Changes in the refractive index of the stroma and its extrafibrillar matrix when the cornea swells. *Biophys J.* 2003;85:2205–2212.
32. Lee D, Wilson G. Nonuniform swelling properties of the corneal stroma. *Curr Eye Res.* 1981;1:457–461.
33. Turss R, Friend J, Reim M, Dohlman CH. Glucose concentration and hydration of the corneal stroma. *Ophthalmic Res.* 1971;2:253–260.
34. Barer R, Joseph S. Refractometry of living cells, 1: basic principles. *Q J Microsc Sci.* 1954;95:399–423.
35. Scarcelli G, Yun SH. Multistage VIPA etalons for high-extinction parallel Brillouin spectroscopy. *Opt Express.* 2011;10913–10922.
36. Scarcelli G, Kim P, Yun SH. Cross-axis cascading of spectral dispersion. *Opt Lett.* 2008;33:2979–2981.
37. Fung YC. *Biomechanics: Mechanical Properties of Living Tissues*. New York: Springer-Verlag; 1993.
38. Maurice DM. The structure and transparency of the cornea. *J Physiol (Lond).* 1957;136:263–286.
39. Komai Y, Ushiki T. The three-dimensional organization of collagen fibrils in the human cornea and sclera. *Invest Ophthalmol Vis Sci.* 1991;32:2244–2258.
40. Jester JV, Winkler M, Jester BE, Nien C, Chai D, Brown DJ. Evaluating corneal collagen organization using high-resolution nonlinear optical macroscopy. *Eye Contact Lens.* 2011;36:260–264.
41. Morishige N, Wahlert AJ, Kenney MC, et al. Second-harmonic imaging microscopy of normal human and keratoconus cornea. *Invest Ophthalmol Vis Sci.* 2007;48:1087–1094.
42. Bueno JM, Gualda EJ, Artal P. Analysis of corneal stroma organization with wavefront optimized nonlinear microscopy. *Cornea.* 2011;30:692–701.
43. Morishige N, Takagi Y, Chikama, T.-i., Takahara A, Nishida T. Three-dimensional analysis of collagen lamellae in the anterior stroma of the human cornea visualized by second harmonic generation imaging microscopy. *Invest Ophthalmol Vis Sci.* 2011;52: 911–915.
44. Teng SW, Tan HY, Sun Y, et al. Multiphoton autofluorescence and second-harmonic generation imaging of the ex vivo porcine eye. *Invest Ophthalmol Vis Sci.* 2006;47:1216–1224.
45. Kling S, Remon L, Perez-Escudero A, Merayo-Lloves J, Marcos S. Corneal biomechanical changes after collagen cross-linking from porcine eye inflation experiments. *Invest Ophthalmol Vis Sci.* 2010;51:3961–3968.
46. Wollensak G, Spoerl E, Seiler T. Stress–strain measurements of human and porcine corneas after riboflavin-ultraviolet-A-induced cross-linking. *J Cataract Refract Surg.* 2003;29:1780–1785.
47. Wollensak G, Aurich H, Pham DT, Wirbelauer C. Hydration behavior of porcine cornea crosslinked with riboflavin and ultraviolet A. *J Cataract Refract Surg.* 2007;33:516–521.
48. Kampik D, Ralla B, Keller S, Hirschberg M, Friedl P, Geerling G. Influence of corneal collagen crosslinking with riboflavin and ultraviolet-A irradiation on excimer laser surgery. *Invest Ophthalmol Vis Sci.* 2010;51:3929–3934.
49. Liu J, Roberts CJ. Influence of corneal biomechanical properties on intraocular pressure measurement: quantitative analysis. *J Cataract Refract Surg.* 2005;31:146–155.
50. Hjortdal JO. Regional elastic performance of the human cornea. *J Biomech.* 1996;29:931–942.
51. Kohlhaas M, Spoerl E, Schilde T, Unger G, Wittig C, Pillunat LE. Biomechanical evidence of the distribution of cross-links in corneas treated with riboflavin and ultraviolet A light. *J Cataract Refract Surg.* 2006;32:279–283.
52. Muller LJ, Pels E, Vrensen G. The specific architecture of the anterior stroma accounts for maintenance of corneal curvature. *Br J Ophthalmol.* 2001;85:437–443.
53. Randleman JB, Dawson DG, Grossniklaus HE, McCarey BE, Edelhauser HE. Depth-dependent cohesive tensile strength in human donor corneas: implications for refractive surgery. *J Refract Surg.* 2008;24:85–89.
54. Mofrad MRK, Kamm RD, eds. *Cytoskeletal Mechanics*. New York: Cambridge University Press; 2006.